Tailor-made dual doping for morphology control of polyaniline chains in cellulose nanofiber-based flexible electrodes: electrical and electrochemical performance

Tailor-made dual doping for morphology control of polyaniline chains in cellulose nanofiber-based flexible electrodes: electrical and electrochemical performance

Tereza Bautkinová[1], Petr Mazúr[1], Gabriela Soukupová[1], Marcela Dendisová[1], Jan Prokeš[2], Marek Jurča[3], Dušan Kopecký[1], Miloslav Lhotka[4], Pavel Ulbrich[5], and Fatima Hassouna[1,*]

[1]Faculty of Chemical Engineering, University of Chemistry and Technology, 166 28 Prague 6, Prague, Czech Republic

[2]Faculty of Mathematics and Physics, Charles University, 180 00 Prague 8, Czech Republic

[3]Centre of Polymer Systems, Tomas Bata University in Zlín, 760 01 Zlín, Czech Republic

[4]Faculty of Chemical Technology, University of Chemistry and Technology, 166 28 Prague 6, Prague, Czech Republic

[5]Faculty of Food and Biochemical Technology, University of Chemistry and Technology Prague, 166 28 Prague 6, Czech Republic

Address correspondence to E-mail: fatima.hassouna@vscht.cz

ABSTRACT

The present study revealed the effect of combining one strong-inorganic and weak-organic protonic acid dopants on the electrical conductivity and electrochemical properties of flexible free-standing composite electrodes based on polyaniline and nanofib-rillated cellulose (NFC) or its carboxylated analog ($CNFC$), synthesized using a bottom-up approach. Hydrochloric acid (HCl) served as a low molecular weight inorganic dopant while phytic acid (PhA) and poly(2-acrylamido-2-methyl-1-propanesulfonic acid) ($PAAMPSA$) were chosen as the organic dopants. Both PhA and $PAAMPSA$ acted as secondary dopants in the dually doped composites through the molecular conformation changes of $PANI$ chains. Synergistic increase in the electrical conductivity is observed for dually doped $PANI$-NFC with the combination of $PAAMPSA$ and HCl in comparison with PhA and HCl. Unlike the PhA, the morphological changes induced by PAAMPSA are more favorable for the enhancement of conductivity. Neither the morphological changes, nor the carboxylation of NFC affected the electrochemical properties of the composites as the specific capacitance values were influenced mainly by the type and the strength of the individual acids. The capacitance values per gram of the dually doped composite with $PAAMPSA$ and HCl increased with the decrease in the NFC or $CNFC$ loading reaching values above 200 F g^{-1} measured at 50 mV·s^{-1} of composite for the 80 wt% $PANI$ content. These results highlight the profound impacts of the secondary dopant in $PANI$ on the performance of $PANI$-based nanocellulose composites.

Introduction

With the rapid increase in energy and power demands for the next-generation of flexible and portable electronics like wearable devices, roll-up displays and photovoltaic cells, considerable efforts have been made to explore flexible, low-cost, lightweight, environmentally friendly and high-performance sustainable energy storage devices [**1, 2**]. Substitution of conventional materials in the fabrication of energy storage devices by renewable materials has been encouraged to tackle issues related to the dependence on fossil fuels and their negative impact on the environment. In this regard, cellulose is the most abundant natural polymer on Earth [**3**]. Compared to regular cellulose substrates, nano-structured cellulose, namely nanofibrillated cellulose (NFC), cellulose nanocrystals and bacterial cellulose, exhibits higher mechanical strength, high aspect ratio, low density, better optical transparence, and smoother and more reactive surface with the potential for tunable functionalization. Those features make the nanocellulose an attractive choice for various applications [**4, 5**]. It can be employed as a matrix for fabrication of flexible composites with some active materials that are intrinsically rigid or brittle. A good example of such brittle materials is electrically conducting polymers (ECP). $ECPs$ like polyaniline ($PANI$) have developed into a promising category of materials for energy storage devices thanks to their relatively high theoretical capacities ($\sim$ 100 to 140 mA h·g^{-1}), rich redox chemistry, versatility as well as lightweight and inexpensiveness [1, 6, 7]. Nevertheless, because of their poor mechanical properties and processability (infusibility and limited solubility in all available solvents), it is very difficult to produce neat ECP films. Flexible free-standing electrically conductive films based on NFC and PANI are very attractive materials for development of high-performance sustainable energy storage devices [8, 9]. Electrical conductivity and supercapacitive behavior of $PANI$ can be influenced by the nature of the dopant [**10,11**]. Doping can be performed by two routes, namely i) redox doping, in which oxidizing or reducing agent add/remove electron to/from polymeric backbone, or ii) protonic acid doping, in which the electron number in the polymer backbone stays unaffected [**11**]. Recent studies showed that in addition to the utilization of an individual (i.e., single) dopant, a secondary doping, as well as the use of dopant combination, can significantly enhance the electrical and electrochemical properties of $PANI$ [**10-12**]. The primary dopant, which can be a molecule or a macromolecule, is capable of changing drastically the electronic, magnetic, optic or/and structural properties of PANI, and leads to a substantial increase in the electrical conductivity [**12**]. On the other hand, the secondary dopant is an apparently inert molecule (e.g., solvent) which can positively affect the above-mentioned properties and is accompanied with further enhancement of the electrical conductivity of $PANI$, even after a complete removal of the secondary dopant. In some cases, it can also further enhance the electrochemical properties [**10-14**]. MacDiarmid et al. demonstrated that the impacts of the secondary dopants are based mainly on the molecular conformation changes of $PANI$ from compact coil to expanded coil [**12**]. Secondary doping of $PANI$ during the synthesis with different combinations of primary/secondary dopant such as sul-fophthalic acid/sodium laurylsulfate [**15**], fluoroboric acid/dodecylhydrogen sulfate [**16**], hydrochloric acid (HCl)/sodium dodecyl sulfate [**17**], HCl/polyacrylic acid [17] and camphorsulfonic acid/citric acid [**10**] has been reported in several studies. They have all reported an enhancement of the electrical conductivity properties of doped $PANI$. Interestingly, apparently inert solvents like m-cresol can also act as a secondary dopant for PANI following similar mechanism of the secondary doping process described above [**12**]. For instance, it has been reported that a solvent casted camphorsulfonic acid-doped $PANI$ using m-cresol (solvent) exhibited 10^3 times higher electrical conductivity than the cast obtained from chloroform [**12**]. Establishment of polar interactions between the polar m-cresol and the polar chains of $PANI$ promotes an expanded open coil conformation of $PANI$ chains.

Despite these considerable scientific efforts made to enhance the properties of $PANI$ and to understand the synergetic effect mechanism of the simultaneous dual doping, secondary doping of $PANI$ in complex systems involving more than one component, i.e., composites, has been barely investigated. According to the available literature, secondary doping has not been explored in flexible free-standing electrically conductive electrodes based on nanocellulose and $PANI$ yet despite the tremendous interest aroused in these materials. The present study reveals the effect of the combinations of one strong-inorganic and weak-organic protonic acid dopants on the electrical and electrochemical properties of composite electrodes based on $PANI$ and NFC or its carboxylated NFC ($CNFC$). To the best of our knowledge, this is the first study, which explored the effect of the dual doping, with the objective to improve the electrical and electrochemical performance of the free-standing NFC-based composites. The composite electrodes were prepared using a bottom-up approach as freestanding flexible films. HCl was selected as a low molecular weight inorganic dopant that is known to yield $PANI$ with high values of electrical conductivity [**18**]. Phytic acid (PhA) and poly(2-acrylamido-2-methyl-1-propanesulfonic acid) ($PAAMPSA$) were chosen as organic acid dopants. PhA can act as a dopant as well as a crosslinker of $PANI$ thanks to the multiple phosphoric acid groups present in its backbone [**19, 20**]. Unlike PhA, $PAAMPSA$ is a polymeric dopant of $PANI$ formed via polymerization of 2-acrylamido-2-methyl-1-propanesulfonic acid ($AAMPSA$). $PAAMPSA$ induces uniform crystalline nanofibrillar morphology of PANI chains [**21**]. A combination of the benefits of these two types of doping acids, namely desired and controlled morphological features provided by organic acids (PhA or $PAAMPSA$) and high electrical conductivity provided by inorganic acid (HCl), was explored with the goal to optimize the electrical and electrochemical performance of the final $PANI/NFC$ and $PANI/\ CNFC$ composite films. The impact of the surface chemistry of the cellulosic fibers (i.e., hydroxyl groups in NFC and carboxyl groups in CNFC) and the composite composition on the structural and morphological features are related performance of the dually doped $PANI$-based composites was also investigated.

Experimental part

Materials

Nanofibrillated cellulose (NFC) was kindly donated by Weidmann Fiber Technology. Aniline (ACS reagent, $>$ 99.5%), 2-acrylamido-2-methyl-1-propanesulfonic acid ($AAMPSA$, 99%), sulfuric acid (H_2SO_4, 95-98%), phytic acid (PhA, 50 wt% solution in water), ammonium persulfate (APS, 98%), 2,2,6,6-Tetramethylpiperidine-1-oxyl radical ($TEMPO$, 98%), sodium hypochlorite solution ($NaClO$, 10 wt%), sodium bromide ($NaBr$) and dimethyl sulfoxide ($DMSO$) were purchased from Sigma Aldrich. Fuming hydrochloric acid (HCl, 37%) was purchased from Merck. All chemicals were used as received without any further purification. All aqueous solutions were prepared using deionized water.

Materials preparation

Synthesis of $PANI$ with various doping acids

Synthesis of $PANI$ was carried out by chemical oxidative route in the presence of one or two acids for individual and dual doping, respectively. Acids, namely HCl, PhA, $PAAMPSA$ (via polymerization of $AAMPSA$), PhA/HCl and $PAAMPSA/HCl$ were used. In a typical $PANI$ synthesis, 300 mg of aniline was dissolved in 60 mL of an aqueous solution of a particular acid(s), to keep the concentration of $PANI$ constant at 0.5 wt% regardless of the doping agent(s) used. The proportions in molar ratios of

aniline/organic co-dopant (i.e., PhA and $AAMPSA$) in the dually doped samples were set to 1:1. Table S1 in the supporting information summarizes the sample designations together with amount of acid(s) dissolved in the reaction medium. The reaction system was cooled down in an ice bath prior to the dropwise addition of 5 mL of APS aqueous solution (0.15 w/w%) to initiate the chemical reaction. The reaction mixture was stirred at 300 rpm overnight. The resulting $PANI$ in a form of dark green precipitate was then filtered and washed several times with deionized water, and subsequently dried at room temperature for several days to obtain dry powder. The PANI powders were labeled as $PANI$(dopant) or $PANI$(co-dopant + dopant) (Table S1).

Synthesis of $PANI - NFC$ composites with various doping acids

The synthesis of individually and dually doped $PANI - NFC$ composites was performed following the same experimental protocol than for $PANI$ powders, with slight modifications. For $PANI - NFC$ composites, 300 mg of NFC and 300 mg of aniline (weight ratio aniline/NFC = 50:50 w/w%) were incorporated in 120 mL aqueous solution of a particular acid(s), adjusting the concentration of $PANI - NFC$ at 0.5 wt% regardless of the employed doping agent(s). Stirring speed was increased to 600 rpm to overcome the higher viscosity caused by the addition of NFC. Table S1 summarizes the sample designations together with amount of acid(s) dissolved in the reaction medium. The reaction system was cooled down in an ice bath prior to the dropwise addition of 5 ml of APS aqueous solution (0.15 wt%). The reaction mixture was stirred at 600 rpm overnight. After the polymerization was completed, the resulting green dark precipitate was washed several times. The washed product was resuspended in 70 mL of deionised water by sonication for 10 min using sonication bath (PS 3000, PowerSonic). Afterward, the suspension was casted on a glass mold with defined shape. The concentration of $PANI$ in the films was set to 2 mgcm-2. The casted materials were dried at room temperature for several days to obtain free standing films with the weight ratio $PANI/NFC$ of 50:50 w/w%. The composites were labeled as $PANI$(-dopant)-NFC or $PANI$(co-dopant + dopant)-NFC (Table S1).

Synthesis of $PANI - NFC$ composites at different $PANI/\ NFC$ ratio

The synthesis of dual-doped $PANI$($PAAMPSA + HCl$)-NFC composites at various $PANI{:}\,NFC$ ratios was performed following the synthetic route described above (see Section "**Synthesis of PANI-NFC composites with various doping acids**"). The amount of NFC was varied while that of aniline was kept constant (300 mg). The amount of $AAMPSA$ was also kept constant (600 mg) and the volume of 1 M HCl aqueous solution was adjusted for each composite (see Table S1). The sample designations are shown in Table S1 where the ratio in w/w% of $PANI$(-$PAAMPSA + HCl$):NFC is denoted at the end of the sample name.

Synthesis of $CNFC$ and their $PANI$-based composites

$CNFC$ was synthesized by TEMPO mediated oxidation of NFC [**22**]. 510 mg of NFC was dispersed in 100 mL of deionized water, and 14.75 mg of TEMPO and 162 mg of NaBr dissolved in 5 mL of deionized water were added. NaOH solution (0.5 M) was used to maintain pH 10.2 all over the reaction. 7 mL of NaClO was then added to initiate the oxidation. The reaction was quenched after 60 min by addition of 2 mL of methanol. The resulting $CNFC$ was washed several times with deionised water in a centrifuge (10,000 rpm for 5 min). The concentration of $-$COOH groups obtained by conductometric titration was 1.56 mmolg^{-1}.

The synthesis of dual-doped $PANI(PAAMPSA + HCl)$-CNFC composites at various $PANI{:}CNFC$ ratios was carried out following the synthetic route used to prepare $PANI(PAAMPSA + HCl)$-NFC (see Section "**Synthesis of PANI-NFC composites at different PANI/NFC ratio**").

Characterization methods

Dispersive Raman spectrometer

Dispersive Raman spectrometer with the microscope InVia Reflex was employed for chemical characterization of samples. Excitation wavelength 785 nm with laser power of 2 mW was used. Ten accumulations taking 30 s were recorded for one acquisition and final spectrum is average of 10 acquisitions.

X-ray photoelectron spectroscopy

X-ray photoelectron spectroscopy analysis was carried out with Omicron Nanotechnology X-ray photoelectron spectroscope (XPS) composed of monochromatic radiation of Al lamp (1486.7 eV) in constant analyzer energy mode. Deconvolution of collected spectra was done using CasaXPS software.

Scanning electron microscopy

Surface and bulk morphology of the films was analyzed using thermo-autoemission scanning electron microscope (SEM) Mira 3 LMH (Tescan Orsay) under 3 kV of accelerating voltage.

Transmission electron microscopy

The morphology of NFC and $CNFC$ at a nanoscale level was analyzed using transmission electron microscope (TEM) 100 kV, model JEM-1010 (JEOL, Ltd.) equipped with CCD camera MegaView III (Olympus Soft Imaging Systems). In short, 10 iL of suspension was deposited on a carbon-coated electron microscopic grid. Sample contrasting was performed using 1 wt% uranyl acetate. The grid was dried and then was introduced into the electron microscope column for analysis.

Electrical conductivity

Room temperature electrical conductivity was determined by a four-point method in van der Pauw arrangement using a Keithley 220 Programmable Current Source, a Keithley 2010 Multimeter as a voltmeter and a Keithley 705 Scanner equipped with a Keithley 7052 Matrix Card. Films were analyzed as prepared, while reference PANI powders were finely grinded and then pressed into pellets with a pressure of 527 MPa for a duration of 5 min. Digital micrometer was used to measure sample thickness before the electrical conductivity measurement. Values of conductivities are provided with approx. 5% accuracy.

Electrochemical characterization

The electrochemical properties were tested in 1 M H_2SO_4 electrolyte. A mercury sulfate reference electrode (MSE) with saturated K_2SO_4 inner electrolyte (0.65 V vs. SHE) and platinum sheet counter electrode were used in a three-electrode arrangement. The electrochemical behavior of the nanocomposites was characterized by cyclic voltammetry (CV) in potential range from - 0.1 to 0.5 V vs. MSE with scan rate of 50 mV s^{-1} and by galvanostatic charging discharging (GCD) at various constant currents. Poten-tiostat/galvanostat/FRA EC-LAB SP-300 (Biologic) is used for these measurements.

The specific capacitance is evaluated from CV experiment following formula **1**:

$$C_{sp} = \frac{\int_{E_{\min}}^{E_{\max}} \frac{I}{v} dE}{(E_{\max} - E_{\min}) \cdot m} \qquad (1)$$

where v is scan rate, m is mass of electrochemically active components in the material, and E_{max} and E_{min} are the chosen boundaries of the integral. Herein, specific capacitance is calculated from cathodic part of CV curve within boundaries from -0.8 V to 0.2 V vs. MSE. The samples were measured in a form of small circles, 6 mm in diameter. Mass of these circles varied from 1 to 2 mg, depending on specific sample.

GCD experiments that were used for establishment of cycling stability of prepared composites were done at controlled current of 2 mA (corresponding to current density of 0.64 $mAcm^{-2}$) in a narrower voltage window from - 1 to 0.1 V vs. MSE in order to avoid hydrolysis of $PANI$.

Tensile testing

Mechanical properties of the composite films were evaluated by tensile tests. Five specimens (20 × 5 mm) were cut from each sample. A micrometer was used to measure their thickness before the test. Measurements were taken at four different positions for each specimen, and the average value was used for the calculation. Tensile test was performed using a universal testing machine (EZ graph, Shimadzu Corporation) with a 100 N load cell and a 0.5 mm min^{-1} strain rate.

Nitrogen physisorption

The specific surface area ($SBET$) was measured on a 3Flex analyzer (Micromeritics, Norcross) using the gas sorption technique. The samples were degassed at 373 K (12 h) prior to N_2 adsorption analysis, in order to obtain a clean surface. The adsorption isotherms were fitted by using the Brunauer-Emmett-Teller (BET) method for specific surface area.

Results and discussion

$PANI - NFC$ composites doped with different acids

All $PANI - NFC$ composites doped with different acids are dark green films with a thickness of approx. 70 μm. Representative photographs of $PANI - NFC$ composite films are shown in **Fig. 1**. All films are mechanically stable and can be rolled up without breaking.

Chemical structure and morphology

Chemical structure of the reference PANI powders and $PANI - NFC$ composite films (**Fig. 1**) doped with various acids was examined by means of Raman spectroscopy and XPS.

Raman spectra of all $PANI$ powders depicted in **Fig. 2**a display the characteristic peaks corresponding to the structure of emeraldine salt, typically at 1510 cm^{-1} (vibrations of $N - H$ in semiquinonoid structures), 1345 cm^{-1} ($C - N^{\cdot +}$? vibrations of delocalized polarons), 1175 cm^{-1} ($C - H$ bending in semiquinonoid units), 878 cm^{-1} ($C - N - C$ out of plane wagging and benzene ring deformations) and 814 cm^{-1} (benzene ring deformations) [**21, 23, 24**]. No structural changes are observed in $PANI - NFC$ composites when compared to the $PANI$ powders regardless of the chemical nature of the doping agent, which is consistent with the formation of emeraldine salt (**Fig. 2**b).

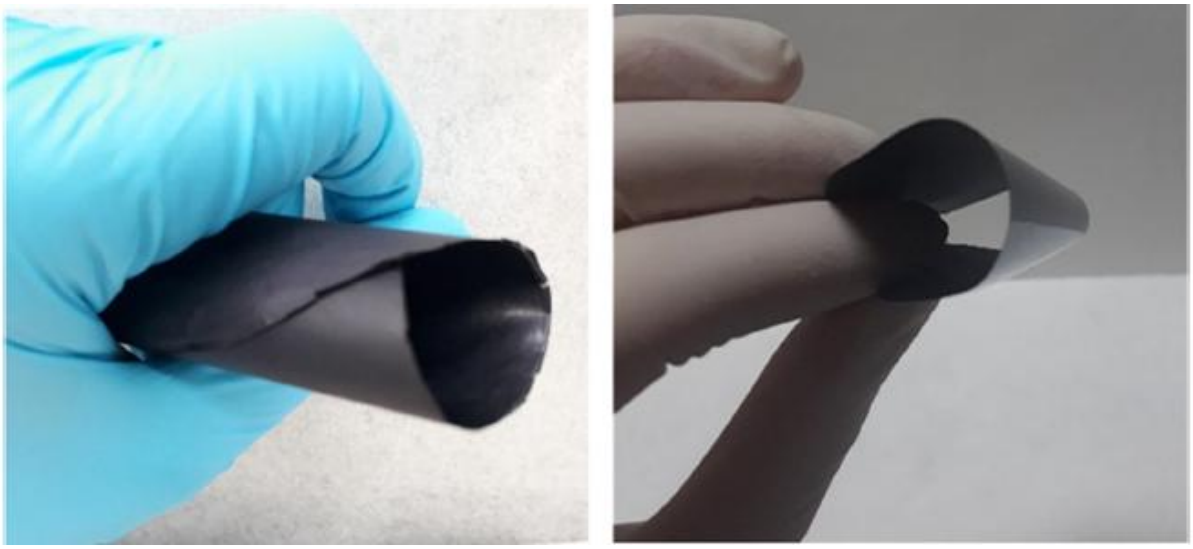

Figure 1 Representative photographs of $PANI - NFC$ composite films prepared with various doping acids.

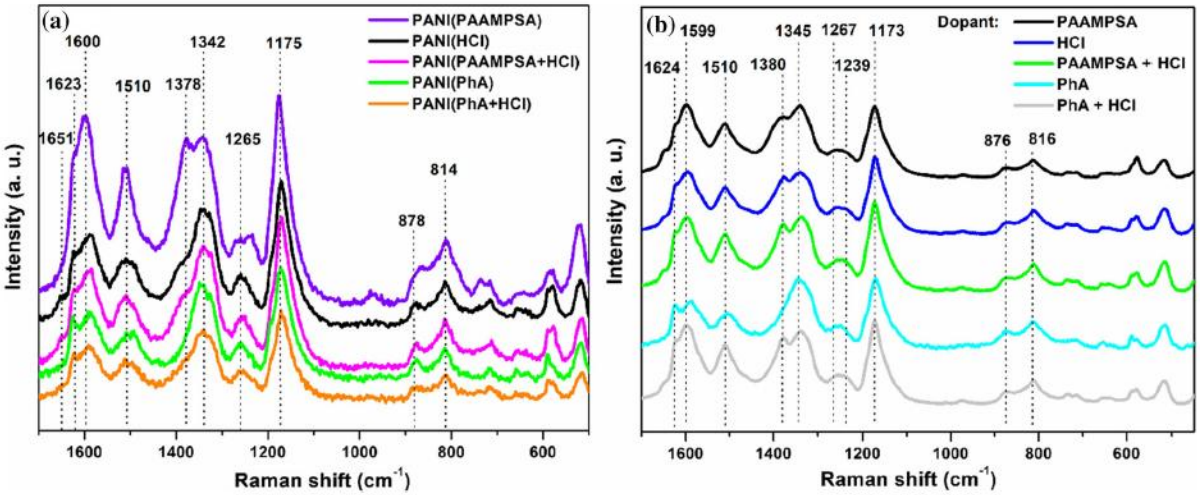

Figure 2 Raman spectra of a $PANI$ powders, and b PANI-NFC composites prepared with various doping acids.

The redox states and protonation degrees in $PANI$ powders and $PANI-NFC$ composites as a function of the doping acid(s) were assessed by means of XPS analysis [**21, 25-27**]. High resolution spectra of nitrogen were deconvoluted into their components in order to determine the redox state of $PANI$ and its protonation levels as a function of the doping acid(s). It can be noticed that the N(1 s) core-level spectra in Figure S1 (see in the supporting information) and Table 1 were deconvoluted into three peaks with maxima at around 399.4 eV, 400.6 eV and 402.3 eV corresponding to nitrogen atoms in secondary amine, semiquinone (delocalized polaron lattice) and proto-nated imine (localized bipolaron), respectively, with a level of protonation of about 40 $\pm$ 5% in all PANI powders, suggesting the formation of $PANI$ emer-aldine salt regardless of the doping acid(s). The chemical nature and the proportion of the different chemical states of nitrogen functionalities in $PANI-NFC$ composites evaluated by fitting the N(1 s) core spectra (Figure S2 in supporting information and **Table 1**) are equivalent to those of their $PANI$ powder analogs. They exhibited a protonation level of 40 $\pm$ 5% comparable to that displayed by the $PANI$ powders.

Table 1 Summary of XPS data of as-synthesized materials

	NH (%)	NH + (%)	NH + = (%)
Binding Energy (eV)	399	400	402
PANI(HCl)	56.9	30.4	12.7
PANI(PAAMPSA)	61.5	29.4	9.1
PANI(PhA)	57.4	30.0	12.6
PANI(PAAMPSA + HCl)	59.5	27.8	12.8
PANI(PhA + HCl)	64.1	24.2	11.7
PANI(HCl)-NFC	60.3	28.4	11.4
PANI(PAAMPSA)-NFC	62.4	23.7	13.9
PANI(PhA)-NFC	65.9	22.0	12.1
PANI(PAAMPSA + HCl)-NFC	53.8	26.7	19.6
PANI(PhA + HCl)-NFC	58.1	30.6	11.3

The formation of doped $PANI$ in $PANI - NFC$ composites is also evident from X-ray diffrac-tograms (Figure S3 in supporting information) where the characteristic peaks at 25.3° and 9.0° are pointed out [**28**], thus indicating that the crystalline structure of $PANI$ is not influenced by the chemical nature of the doping acids. The characteristic peaks of NFC crystalline structure corresponding to cellulose Iβ are also detected at 15.5°, 16.8°, 20.4°, 22.7° and 34.7° [**29**]. Therefore, the structural properties revealed by Raman spectroscopy, XPS and XRD indicate that on one hand NFC does not affect the protonation levels of $PANI$ and on the other hand all selected acids act as good doping agents.

Impact of the chemical nature of the doping acid(s) on the morphological and textural features of $PANI - NFC$ composites was examined. SEM pictures of individually and dually doped $PANI - NFC$ composites are shown in **Fig. 3**. In comparison with the fibrillar morphology of pristine NFC, NFC fibers are thoroughly covered by $PANI$ in all $PANI - NFC$ composites. Apart from this, morphological differences can be observed. While in all composites globular-like morphology of $PANI$ on the surface of NFC fibers is revealed, dissimilarities in the shape of those globules and their compactness at a nano-scale level can be associated with the type of the dopant. The morphology of $PANI(HCl) - NFC$ reveals a high compactness of the globular objects, whereas in $PANI(-PAAMPSA) - NFC$ and $PANI(PhA) - NFC$ a well-defined globular-like objects of about 200 nm on the surface of NFC are formed. Interestingly the morphology of the dually doped $PANI - NFC$ composites $PANI(PAAMPSA + HCl) - NFC$ and $PANI(PhA + HCl) - NFC$ is a result of a combination of the morphologies caused by each individual dopant. Indeed, the surface of NFC fibers in $PANI(PAAMPSA + HCl) - NFC$ and $PANI(PhA + HCl) - NFC$ is covered by much less defined spiky globular-like structures, due to their higher compactness/coalescence as compared to their HCl-free analogs.

This dopant(s)-dependent morphological features observed by SEM are correlated with the textural differences observed between the components as can be seen in Figure S4 and **Table 2**. Interestingly, based on BET model, all composites exhibited one type of pores with comparable total pore volume, except for $PANI(HCl) - NFC$. $PANI(HCl) - NFC$ did not display any detectable porosity, hence confirming its high compactness. Nitrogen physisorption isotherms also indicated that the BET surface area (S_{BET}) is the lowest for the composite doped with HCl and the highest for those doped with PhA or $PAAMPSA$. Intermediate values of S_{BET} were recorded for the dually doped composites. The increase in the S_{BET} in the presence of organic acids can be correlated with the morphological changes induced by the latter. $PANI$ crosslinked with phytic acid can ensure higher S_{BET} [**30**]. Indeed, being a crosslinker of $PANI$ thanks to the multiple phosphoric acid groups present in its backbone [**19**], PhA can lead to the formation of well-defined $3D$ nanostructures and induce porosity [**20**]. On the other side, owing to its macromolecular structure $PAAMPSA$ can act as side chains when $PANI$ chains are arranged into crystalline structure. $PAAMPSA$ side chains follow the backbone's arrangement and form a layer between the lattices of $PANI$. This causes the decrease in d-spacing, and thus an increase in the S_{BET} [**31**]. Both PhA and $PAAMPSA$ acted as secondary dopants in the dually doped composites through the macromolecular rearrangements of $PANI$ chains [**12**].

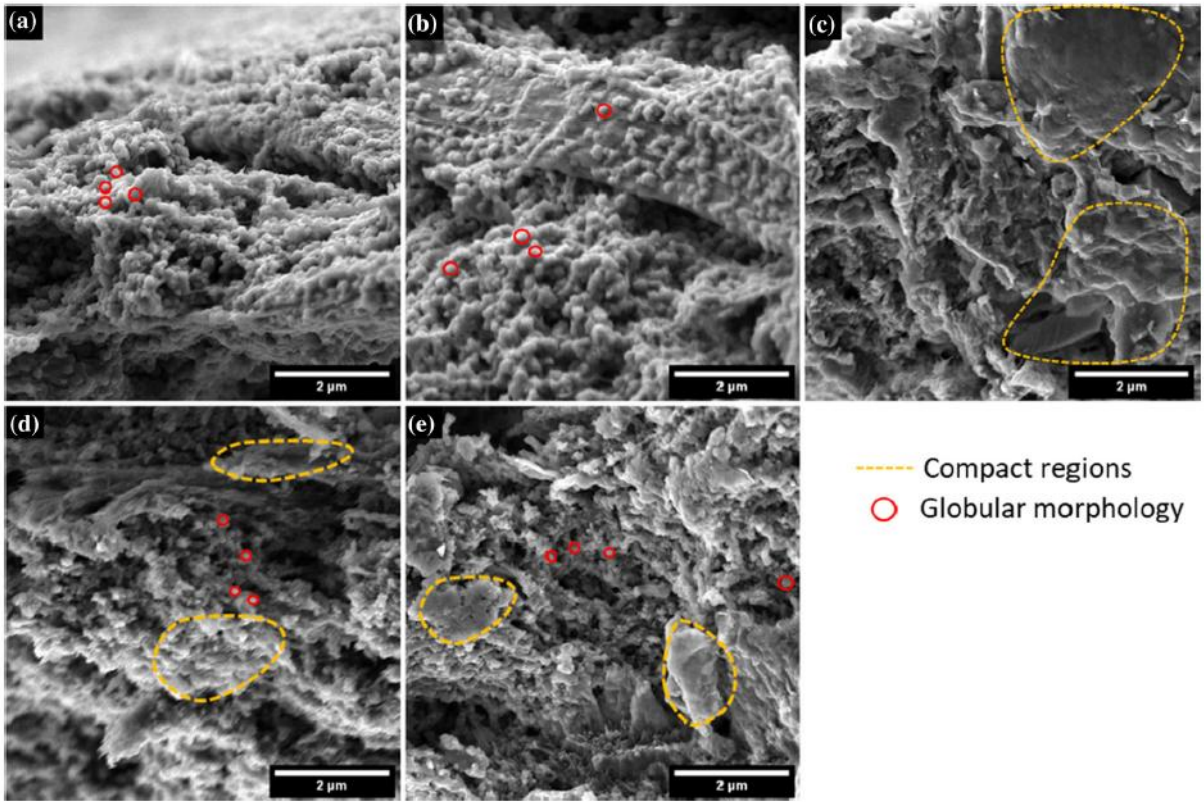

Figure 3 SEM micrographs of $PANI-NFC$ composites doped with various acids: a $PANI(PAAMPSA)-NFC$, b $PANI(PhA)-NFC$, c $PANI(HCl)-NFC$, d $PANI(PhA\ +\ HCl)-NFC$, and e $PANI(PAAMPSA\ +\ HCl)-NFC$.

Table 2 Textural properties of $PANI-NFC$ composites doped with various acids

Sample name	S_{BET} ($m^2 \cdot g^{-1}$)	Total pore volume ($cm^3 \cdot g^{-1}$)
PANI(PAAMPSA)-NFC	17.8	0.035
PANI(PhA)-NFC	17.5	0.035
PANI(HCl)-NFC	9.4	Low porosity
PANI(PhA + HCl)-NFC	13.7	0.039
PANI(PAAMPSA + HCl)-NFC	13.8	0.043

Electrical and electrochemical properties

$PANI-NFC$ composites doped with weak-organic acids, i.e., PhA and $PAAMPSA$, display much lower electrical conductivities compared to the solely HCl-doped composite (**Fig. 4**a). The electrical conductivity is sorted in this direction: $PAAMPSA$ (0.01 S·cm^{-1})$-<$ PhA (0.32 S·cm^{-1}) $<$ HCl (2.43 S·cm^{-1}). The conductivity value of the dually doped $PANI-NFC$ with PhA and HCl (2.28 S·cm^{-1}) is comparable to that of the individually doped $PANI-NFC$ with HCl, thereby indicating that HCl is the main dopant for $PANI$. Synergistic increase in the conductivity is however observed for dually doped $PANI-NFC$ with the combination of $PAAMPSA$ and HCl (3.43 S·cm^{-1}) compared to the corresponding conductivity values of both individually doped $PANI-NFC$. This phenomenon of two dopants synergy has been already described in literature for pristine $PANI$ [**10-12**], but no mechanism explaining this phenomenon has been established yet. According to Bhandari et al. [**10, 11**], a variation of charge densities takes place along the $PANI$ chains when two doping acids are used, thus facilitating intermolecular charge transport.

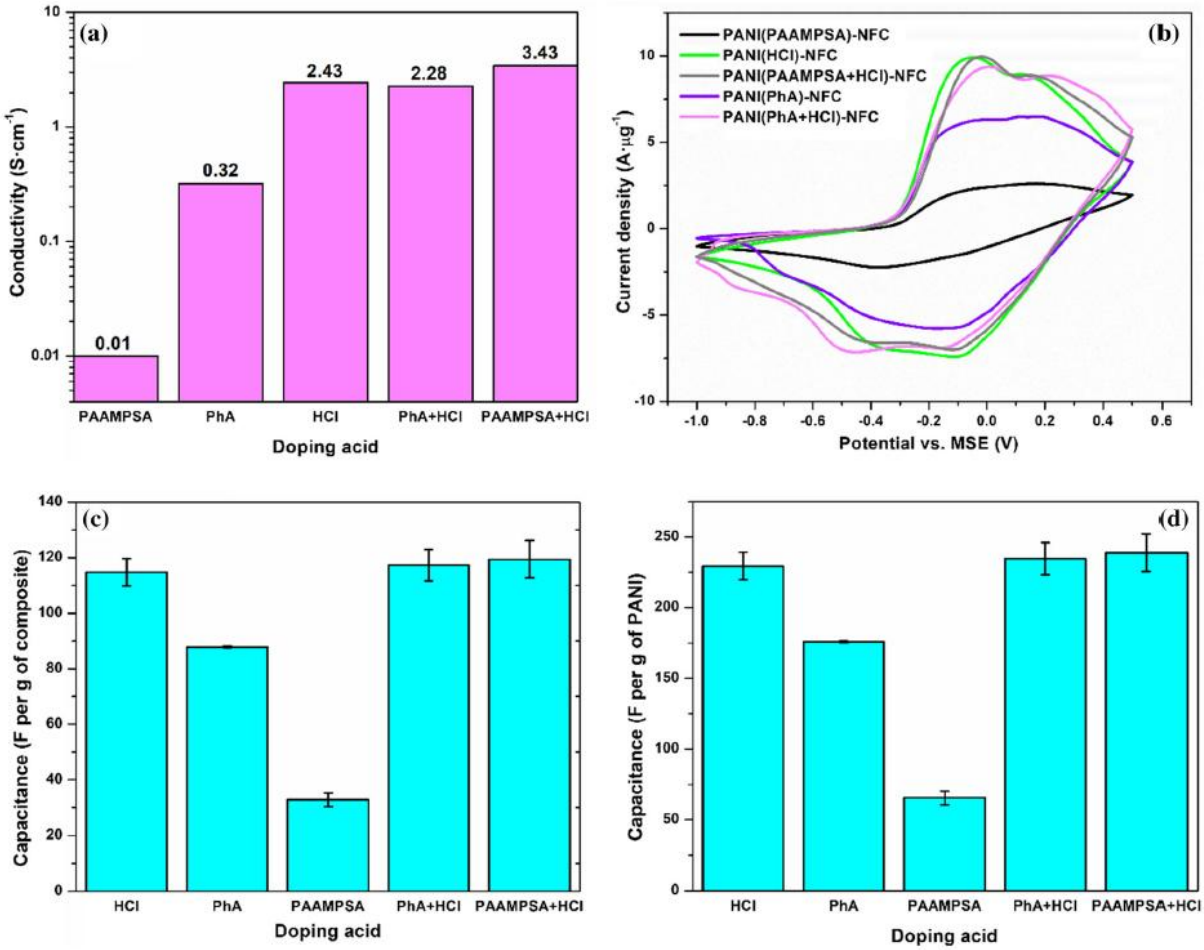

Figure 4 a Electrical conductivities, b cyclic voltammograms of the composite films in 1 M H_2SO_4 at 50 mV·s^{-1} scan rate, c specific capacitances in F per g of composite, and d specific capacitances in F per g of $PANI$ evaluated from CV measurements of $PANI - NFC$ composites doped with various acids.

Nonetheless, this hypothesis has not been further verified. Another hypothesis described by MacDiarmid et al. is based on the concept of secondary doping [**12**]. A secondary dopant is an apparently inert substance (e.g., solvent) that increases the resulting conductivity of already doped conductive polymer. The secondary dopant causes conformational changes in the polymer, which result in enhancement of conductivity through more effective π-conjugation. When secondary dopant is removed from the system, the changes persist. In our composites, the role of the secondary dopant would be taken by $PAAMPSA$. Unlike PhA, the conformational changes induced by $PAAMPSA$ are probably more favorable for the enhancement of conductivity through more effective π-conjugation [**31**]. Indeed, as above mentioned, it is well-known that $PAAMPSA$ can affect the crystalline morphology of $PANI$ owing to its macromolecular structure, low glass transition temperature, and acidic nature. [**21, 32**]. $PAAMPSA$ can act as side chains when PANI chains are arranged into crystalline structure. $PAAMPSA$ side chains follow the backbone's arrangement and form a layer between the lattices of $PANI$, [**31**] which could promote molecular conformation changes of $PANI$ from compact coil to expanded coil. [**12**]. In $PANI(-PAAMPSA + HCl) - NFC$, morphological and textural changes of $PANI$ induced by the secondary dopant, i.e., $PAAMPSA$ through the macromolecular rearrangements of $PANI$ chains was followed by the enhancement of the electrical conductivity. The electrical conductivity enhancement cannot be attributed to a higher degree of doping in the presence of $PAAMPSA + HCl$ since XPS analysis clearly showed that all composites exhibited similar protonation level around 40% whatever the nature of the dopant. Therefore, it is more likely that the

macromolecular rearrangements of $PANI$ chains induced by $PAAMPSA$ was responsible for the conductivity enhancement through more effective π-conjugation in $PANI$ expanded coil as supported by the studies of MacDiarmid et al. [**12**]

The electrochemical behavior of $PANI - NFC$ composites analyzed by cycling voltammetry (CV) is illustrated in Figure S5 and **Fig. 4**b, c and d. Qualitatively, the cyclovoltammograms of $PANI - NFC$ composites and $PANI$ powders are different (Figure S5). $PANI$ powder-based electrodes show all the characteristic peaks of $PANI$: transition between leucoemeraldine and emeraldine (R1 and O1) at lower potentials between - 1.0 and 0.0 V vs. MSE and also transition between emeraldine and pernigrani-line (R2 and O2) at higher potentials between 0.2 and 0.5 V vs. MSE and broad oxidation and reduction peaks (R3 and O3) around 0.0 V vs. MSE indicating quinone/hydroquinone redox switching [**33**]. On the contrary, in the case of $PANI - NFC$ composites, the current peaks are much less pronounced and convoluted together. This most likely relates to the more complex $3D$ structure of the composite since $PANI$ redox switching is controlled by the diffusion of acid molecules from the electrolyte bulk, the porous structure hindering the mass transport can result in a non-homogeneous potential distribution and broader current peaks [**34**]. Redox potential distribution can be also caused by interactions among the redox centers [**34, 35**], in this case, NFC could be mediating a specific chemical environment that can promote different interactions among the $PANI$ chains. The electrochemical performance of all $PANI - NFC$ composites is depicted in **Fig. 4**b, c and d. As can be observed, all three composites that contain HCl (i.e., $PANI(HCl) - NFC, PANI(PhA + HCl) - NFC$ and $PANI(PAAMPSA + HCl) - NFC$) as a dopant reach very similar peak current densities in the CV experiments and thus equivalent specific capacitances of $\sim$ 120 F per g of composite. The synergetic improvement in the electrical conductivity observed for the composite doped with $PAAMPSA + HCl$ is not reflected in the pseudocapacitive behavior of the latter. On the other hand, the composites doped solely with $PAAMPSA$ or PhA exhibited inferior specific capacitance, i.e., $\sim$ 33 and 88 F per g of composite, respectively. These results indicate that the specific capacitances of the composites are correlated with the doping strength of the individual acids [**36, 37**]. The morphological and textural features induced by the secondary dopants ($PAAMPSA$ or PhA) by the enhancement of the S_{BET} do not affect the specific capacitances of the composites (see **Fig. 4**c and d and **Table 2**). The textural changes induced by the secondary dopant are probably not sufficient (i.e., S_{BET} is not substantially increased) to affect the electrochemical properties. Based on the rational screening of a suitable doping acid for $PANI$ in $PANI - NFC$ composites, the combination of a polymeric acid, i.e., $PAAMPSA$, with strong inorganic acid, i.e., HCl, is optimal as HCl confers to the composite higher conductivity while $PAAMPSA$ allows improving the mechanical properties, the dispersibility in water besides its ability to protonate $PANI$ even in media of higher pH [**38, 39**].

$PANI$-based composites doped with $PAAMPSA - HCl$: impact of the composition

Chemical structure and morphology

The effect of mass ratio between $PANI$ and cellulose matrices (i.e., NFC or $CNFC$) on the chemical structure of $PANI$ was examined by Raman spectroscopy (**Fig. 5**a and b) and XPS (Figure S6 and Figure S7). All composites ($PANI(PAAMPSA + HCl) - NFC$ and $PANI(PAAMPSA + HCl) - CNFC$) at different ratios $PANI$ to NFC or $CNFC$ exhibited very similar spectral features in accordance with the formation of emeraldine salt. According to the deconvolution of the N(1 s) core level spectra (Figure S6 and **Table 3**), all composites exhibited a protonation level of 40 $\pm$ 5% comparable to that of $PANI(PAAMPSA + HCl)$ powder. Interestingly, the deconvolution of the C(1 s) core level spectra for all composites (Figure S7 and Table S2) show that the proportion of $C - O/C - N$ at 286.5 eV is

the highest (i.e., 44 $\pm$ 3%) in the composites containing the lowest content of $PANI(-PAAMPSA + HCl)$, i.e., 40 wt%. At higher PANI(PAAMPSA + HCl) content ($\geq$ 50 wt%) the proportion of $C - O/C - N$ remains constant at 24 $\pm$ 3%.

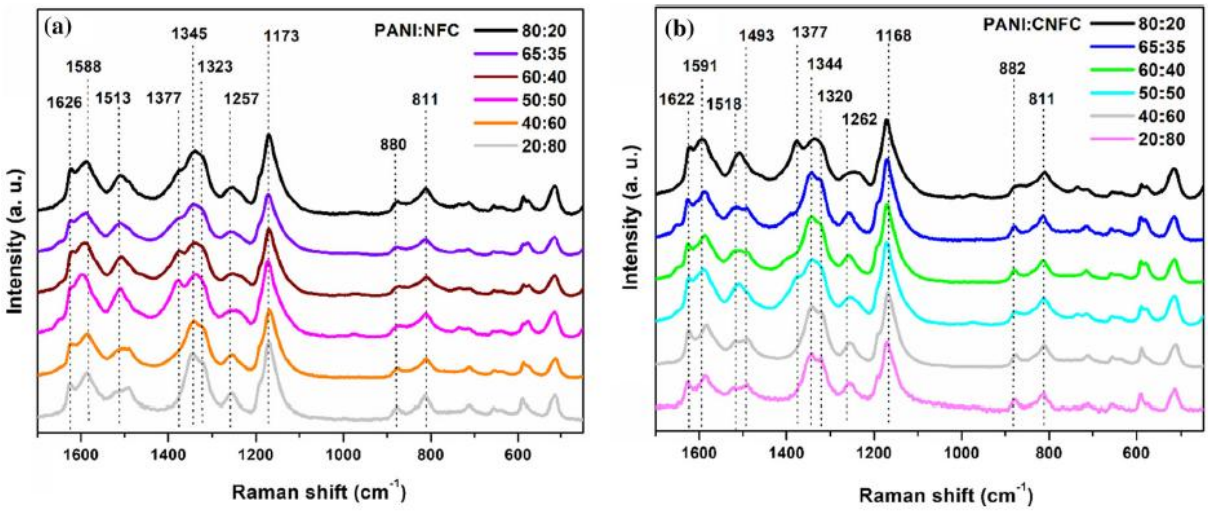

Figure 5 Raman spectra of a $PANI - NFC$, and b $PANI - CNFC$ composites doped with $PAAMPSA - HCl$ at different $PANI$ to NFC or $CNFC$ ratios.

Table 3 Summary of XPS data of as-synthesized materials

	NH (%)	NH + (%)	NH + = (%)
Binding Energy (eV)	399	400	402
PANI(PAAMPSA + HCl)-NFC_40:60	62.7	18.4	19
PANI(PAAMPSA + HCl)-CNFC_40:60	58.5	20.4	21.1
PANI(PAAMPSA + HCl)-NFC_50:50	53.8	26.7	19.6
PANI(PAAMPSA + HCl)-CNFC_50:50	63.4	21.0	15.6
PANI(PAAMPSA + HCl)-NFC_60:40	57.6	25.5	16.9
PANI(PAAMPSA + HCl)-CNFC_60:40	60.4	21.9	17.8
PANI(PAAMPSA + HCl)-NFC_65:35	66.3	23.6	10.1
PANI(PAAMPSA + HCl)-CNFC_65:35	59.5	25.9	14.6
PANI(PAAMPSA + HCl)-NFC_80:20	59.4	27.5	13.2
PANI(PAAMPSA + HCl)-CNFC_80:20	55.9	24.4	19.7

The decrease in the amount of $C - O/C - N$ with the increase in PANI loading correlates with a higher coverage of the surface of NFC or $CNFC$ with $PANI$ since a significant proportion of $C - O/C - N$ can come from NFC or $CNFC$ surface if the latter is not fully covered like in the case of $PANI(PAAMPSA + HCl) - NFC$ at a ratio of 40:60. The maximum coverage of the surface of NFC or $CNFC$ is achieved at a content of $PANI(PAAMPSA + HCl)$ higher or equal to 50 wt.%. As a consequence of the surface oxidation of $CNFC$, an additional peak appeared at 189 eV corresponding to $-COOH$ after deconvolution of the C(1 s) core level spectra for $PANI(PAAMPSA + HCl) - CNFC$ composites. In short, the polymerization of $PANI$ in the emeraldine salt form is not affected by the carboxylation of the NFC fibers.

SEM images of $PANI(PAAMPSA + HCl) - NFC$ and $PANI(PAAMPSA + HCl) - CNFC$ composites are shown in **Figs. 6** and **7**, respectively. Globally, the composites prepared from $CNFC$

have a more compact structure compared to their NFC-based counterparts. This morphology is a result of the defibrillation of cellulose fibers after $TEMPO$ oxidation treatment as evidenced by TEM analysis. (Figure S8). TEM images highlight a finer structure and higher degree of defibrillation in $CNFC$ compared to NFC. This was corroborated by the excellent colloidal stability of $CNFC$ in aqueous medium.

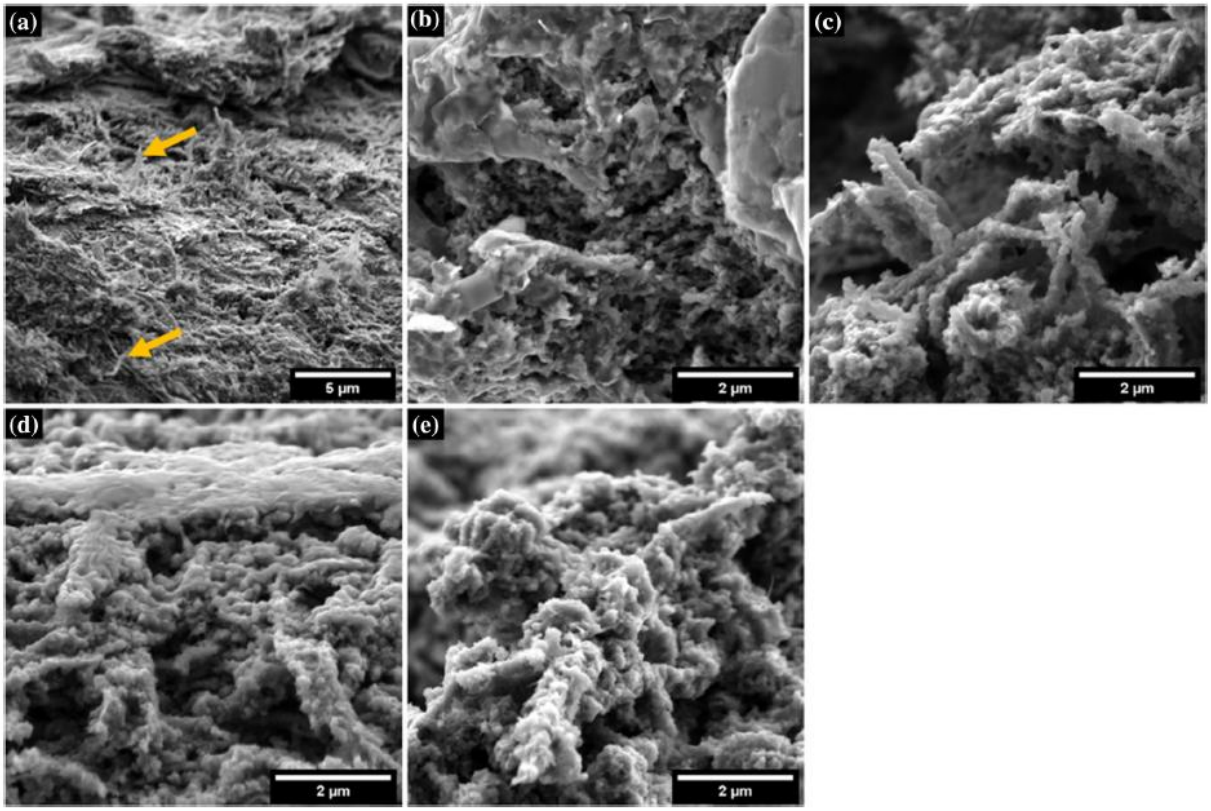

Figure 6 The SEM micrographs of $PANI(PAAMPSA\ +\ HCl) - NFC$ composites at a ratio $PANI$ to NFC: a 40:60, b 50:50, c 60:40, d 65:35 and e 80:20. ⟵: The arrows point to the presence of naked cellidosic fibers in some composites.

Consequently, the spiky globular-like structures of $PANI(-PAAMPSA\ +\ HCl)$ covering $CNFC$ are smaller and the coating layer is finer than in the case of NFC. As a consequence of this morphology, the S_{BET} is close to zero in the composites prepared from $CNFC$ (**Table 4**) unlike those processed from NFC. NFC −based composites show much more prominent fibrillar morphology with cellulose fibrils covered by globular-like structures of $PANI(PAAMPSA\ +\ HCl)$ layer.

At lower amount of $PANI(PAAMPSA\ +\ HCl)$ (i.e., B 50 wt% $PANI(PAAMPSA + HCl)$), naked cellulosic fibers are visible in both types of composites. These morphological observations are in a good agreement with XPS results. S_{BET} of NFC −based composites increases with the increase in $PANI(-PAAMPSA + HCl)$ content up to 50 wt%., which corresponds to the maximum coverage of NFC surface.

Electrochemical behavior of $PANI(PAAMPSA\ +\ HCl) - NFC$ *and* $PANI(PAAMPSA\ +\ HCl) - CNFC$ *composites*

Electrochemical behavior of $PANI(PAAMPSA + HCl) - NFC$ and $PANI(PAAMPSA + HCl) - CNFC$ composites as a function of the composition is illustrated in **Fig. 8**. Cyclic voltammetry was carried out in a three-electrode setup measurement at 50 mV·s^{-1} scan rate to evaluate the effect of

ratios between $PANI$ and NFC in the prepared composites on their charge storage properties. The results are summarized in the histograms (**Fig. 8**a). According to expectations the capacitance per gram of the whole composite shows an increasing trend with decreasing amount of NFC, which is consistent with the fact that each composite contains the same mass of PANI (thus, wt. ratio of PANI:NFC increases). An interesting conclusion can be drawn from the results when the values of capacitances are taken relative to the mass of $PANI$ as is shown in **Fig. 8**b.

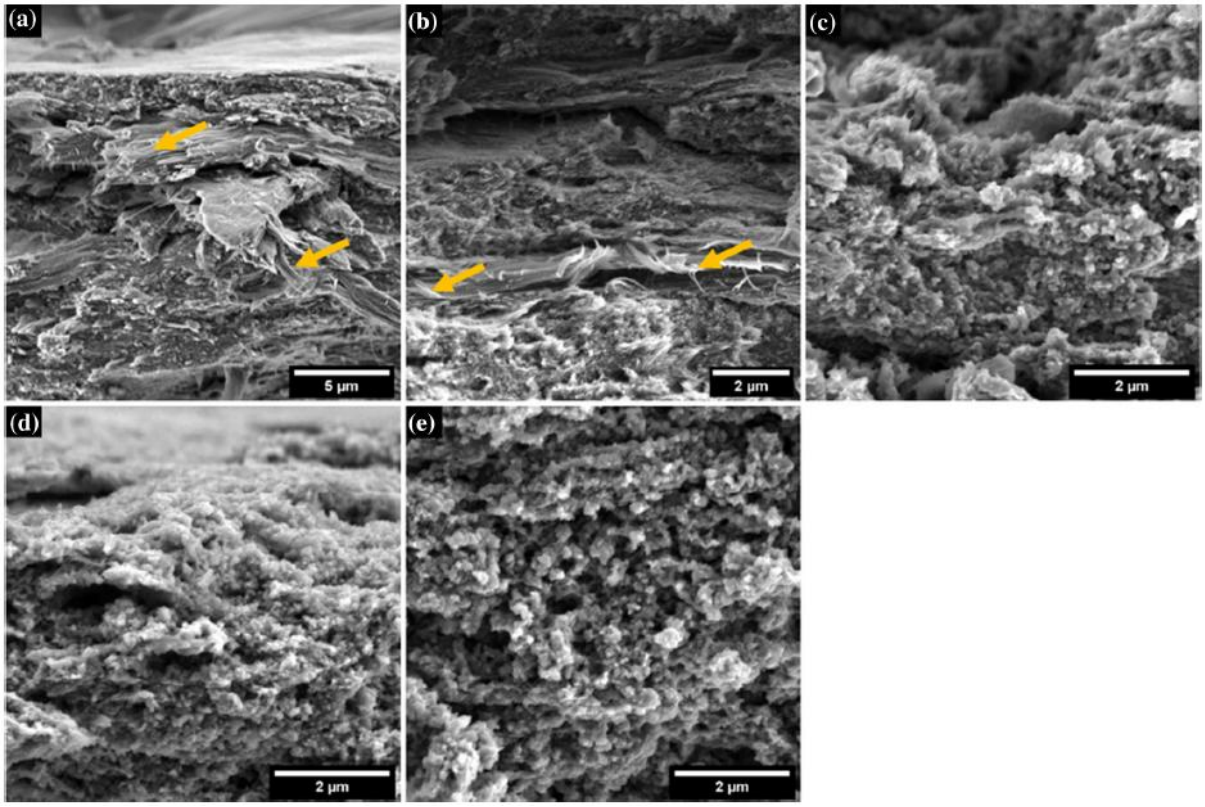

Figure 7 The SEM micrographs of $PANI(PAAMPSA\ +\ HCl) - CNFC$ composites at a ratio $PANI$ to $CNFC$: a 40:60, b 50:50, c 60:40, d 65:35 and e 80:20. ⟶: The arrows point to the presence of naked cellidosic fibers in some composites.

Table 4 Textural properties of $PANI(PAAMPSA +\ HCl) - NFC$ and $PANI(PAAMPSA +\ HCl) - CNFC$ composites

Sample name	S_{BET} ($m^2 \cdot g^{-1}$)
PANI(PAAMPSA + HCl)-NFC_40:60	5.0
PANI(PAAMPSA + HCl)-NFC_50:50	13.8
PANI(PAAMPSA + HCl)-NFC_60:40	13.5
PANI(PAAMPSA + HCl)-CNFC_50:50	0.5

It is clear that the charge storage properties of these composites are not influenced by the amount of cellulose matrices or the type of the matrix in case of all composites, except for the samples with lowest loading of $PANI$. In other words, the degree of $PANI$ utilization is comparable for all composites. This trend can be connected to the surface coverage of the cellulose fibers with $PANI$. The comparison of the electrochemical results with nitrogen physisorption isotherms (**Table 4**) suggest that there is no correlation between SBET evaluated from physisorption measurements and capacitance. According to BET, $PANI(PAAMPSA +\ HCl) - CNFC$_50:50 is a very compact and non-porous material (with low S_{BET} of 0.5 $m^2\ g^{-1}$) while its capacitance is comparable to more porous films based on non-carboxylated NFC with much higher S_{BET} (such as $PANI(PAAMPSA + HCl)$-

NFC_50:50 providing 13.8 $m^2\ g^{-1}$). This can mean that the charge storage occurs at the superficial layer of the composite and that the bulk is not utilized in any way, probably because of the non-porosity of the composites according to the nitrogen physisorption isotherms.

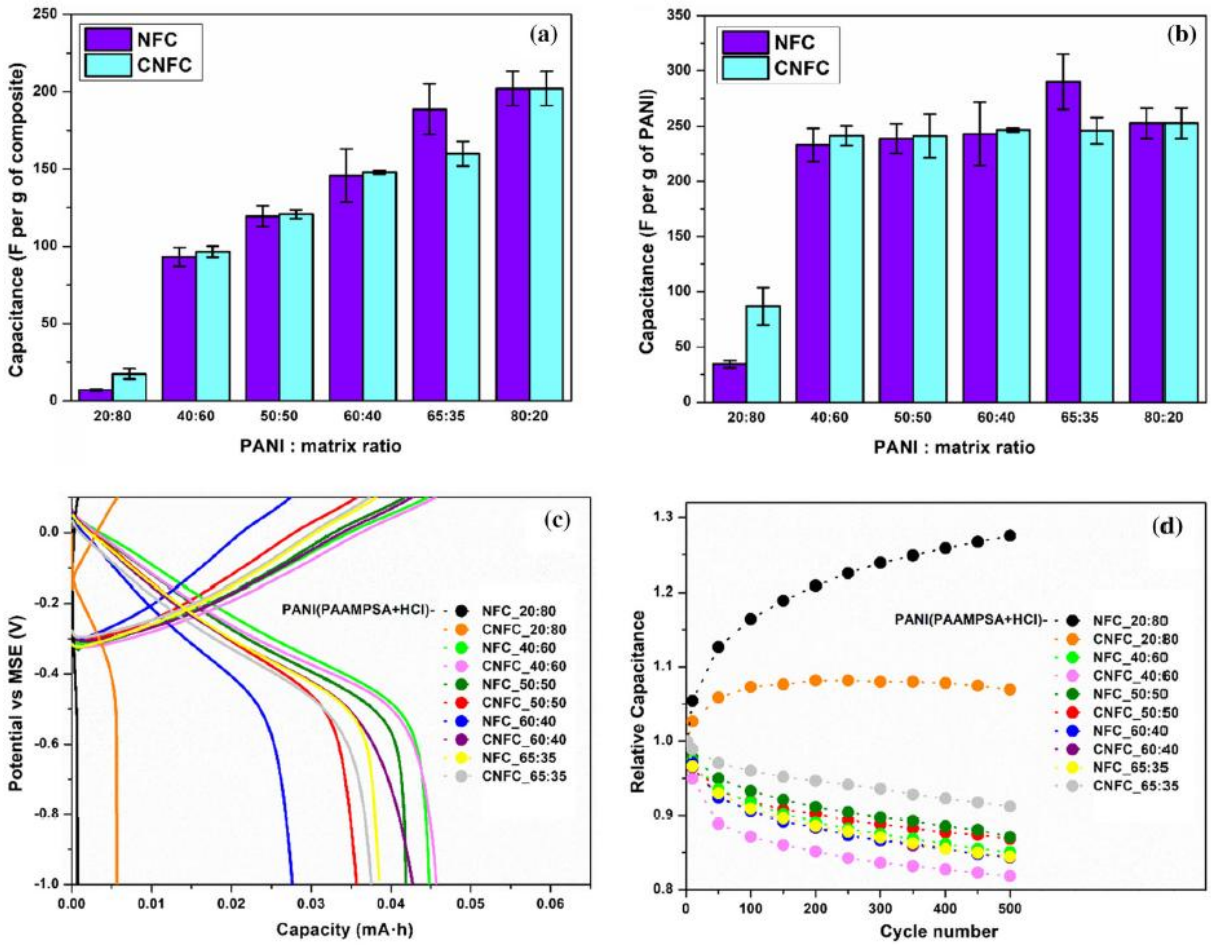

Figure 8 a The specific capacitances in F per g of composite evaluated from CV measurements at 50 mV·s^{-1} for various $PANI/NFC$ or $CNFC$ ratios; **b** specific capacitances in F per g of $PANI$ evaluated from the CV measurements at 50 mV·s^{-1} for various $PANI/NFC$ or $CNFC$ ratios; **c** potential dependence on charge-discharge capacity evaluated from GCD experiments at 0.64 mA·cm^{-2} in the potential window from — 1 V to 0.1 V vs. MSE; **d** Relative specific capacitance of the composite films as a function of the number of cycles evaluated form the GCD experiments.

Therefore, incomplete surface coverage of NFC or $CNFC$ fibers would lead to decrease in charge storage capability. However, we have to be aware that the S_{BET} values for all the composites are relatively small when compared to standard supercapacitive electrodes based on activated carbons [**40**]. The enhancement in electrode-electrolyte area (e.g., by incorporation of high surface area carbon fillers), thus can be used to increase the charge storage capacity of the material.

The mid-term cycling stability of the composites upon the simulated electrochemical load was probed by GCD experiments in three-electrode set-up. The composites were subjected to 500 cycles at controlled current of 2 mA (corresponding to current density of 0.64 mA·cm^{-2}) in a potential window from — 1 to 0.1 V vs. MSE. The used potential window encompasses only the leucoemeraldine-emeraldine redox transition to avoid excessive composite degradation by hydrolysis of $PANI$. An example of a chargingdischarging curve that was used for capacitance evaluation can be seen in **Fig. 8**c. The charge-discharge plateaus corresponding to redox transition are located in the potential range between 0.1 and - 0.5 V vs. MSE, which is in good agreement with the CV measurements (**Fig. 4**).

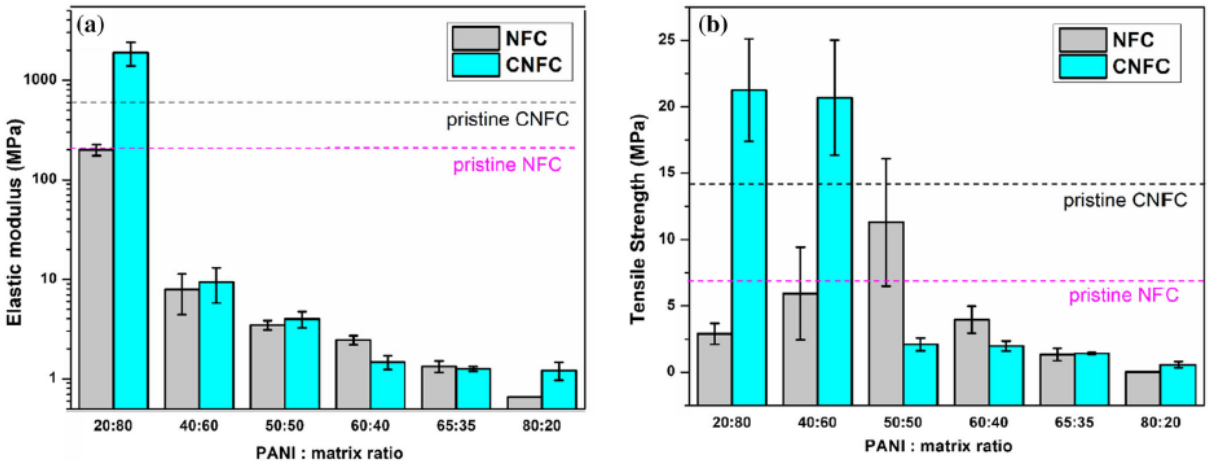

Figure 9 a Elastic modulus and **b** ultimate tensile strength of $PANI(PAAMPSA + HCl) - NFC$ and $PANI(PAAMPSA + HCl) - CNFC$ composites at various $PANI$ to NFC or $CNFC$ ratios as a function of composition.

The evolution of capacitance for the composites is depicted in **Fig. 8**d. All composites, except for those with the lowest loading of $PANI$, show very similar cycling stability-after 500 cycles, the capacitance decreased by about 15% of the initial value. Interestingly, composites with the lowest loading of $PANI$ show an increasing trend of capacitance with number of cycles. This phenomenon could be caused by the inhomogeneity of the composite. Incomplete coverage of the fibers with $PANI$ exposes the highly hydrophilic cellulose to the aqueous electrolyte. Gradual wetting of the fibers can then lead to exposing more of the PANI to the electrolyte, thus increasing the $PANI$ utilization and, in turn, the capacitance of the film.

Mechanical properties of $PANI(PAAMPSA + HCl) - NFC$ and $PANI(PAAMPSA + HCl) - CNFC$ composites

Enhanced mechanical strength and elastic modulus are displayed by the composites with the increased loading of NFC or $CNFC$ as can be seen in **Fig. 9** thanks to the outstanding mechanical features of NFC and $CNFC$. For instance, the composites containing more than 50 wt% NFC or $CNFC$ loading exhibited the highest tensile strength and elastic modulus. In this loading range, $CNFC$ −based composites displayed improved mechanical properties compared to their NFC analogs, thanks to the finer structure and higher degree of defibrillation of $CNFC$ after $TEMPO$ oxidation treatment (Figure S8). In addition, all composites containing higher than 35 wt% loading of NFC or $CNFC$ can be readily rolled up thanks to their high flexibility as both cellu-losic matrices act as a mechanical skeleton capable of high deformations. Abundant hydroxyl and car-boxylate groups present on the surface of NFC or $CNFC$ can interact with $PANI$, and hence may be responsible for the enhancement in the mechanical properties of the composites.

Conclusions

The present study shed the light on the effect of the dual doping of $PANI$ chains via combination of primary (HCl) and secondary (PhA or $PAAMPSA$) dopants in NFC −based flexible pseudo-capacitor electrodes on the morphological, textural and related electrical and electrochemical properties. Both

PhA and $PAAMPSA$ induced morphological and textural changes (increase in the S_{BET}) in the dually doped $PANI - NFC$ composites. Synergistic increase in the electrical conductivity in the case of the dually doped $PANI - NFC$ with $PAAMPSA$ and HCl (i.e., $PANI(-PAAMPSA + HCl) - NFC$) was correlated with a more favorable morphological changes in the composites. Interestingly, the morphological and textural features induced by the secondary dopants ($PAAMPSA$ and PhA) by the enhancement of the specific surface area do not significantly affect the capacitances of the composites evaluated from electrochemical measurements. These were rather correlated with the doping strength of the individual acids. Despite the significant difference in their S_{BET}, the electrochemical behavior of the composites $PANI(PAAMPSA + HCl) - NFC$ and $PANI(PAAMPSA + HCl) - CNFC$ were comparable and the utilization of $PANI$ for charge storage was not significantly affected by the composition of the film (weight ratio of the constituents) or nature of NFC matrix. While the $TEMPO$ oxidation of NFC surface (i.e., $CNFC$) does not affect the electrical and the electrochemical performance of the dually doped composite films, it does enhance the mechanical properties of the latter by acting as a mechanical skeleton capable of higher deformations as compared to NFC.

References

[1] Nyholm L, Nystrom G, Mihranyan A, Stromme M (2011) Toward flexible polymer and paper-based energy storage devices. Adv Mater 23(33):3751-3769

[2] Nishide H, Oyaizu K (2008) Toward flexible batteries. Science 319(5864):737-738

[3] Du X, Zhang Z, Liu W, Deng Y (2017) Nanocellulose-based conductive materials and their emerging applications in energy devices-A review. Nano Energy 35:299-320

[4] Moon RJ, Martini A, Nairn J, Simonsen J, Youngblood J (2011) Cellulose nanomaterials review: structure, properties and nanocomposites. Chem Soc Rev 40(7):3941-3994

[5] Siqueira G, Bras J, DufTesne A (2010) Cellulosic bionanocomposites: a review of preparation properties and applications. Polymers 2:728-765

[6] Snook GA, Kao P, Best AS (2011) Conducting-polymer-based supercapacitor devices and electrodes. J Power Sources 196(1):1-12

[7] Yan H, Chunyi Z (2017) Functional flexible and wearable supercapacitors. J Phys D Appl Phys 50(27):273001

[8] Wang Z, Carlsson DO, Tammela P, Hua K, Zhang P, Nyholm L, Stromme M (2015) Surface modified nanocellulose fibers yield conducting polymer-based flexible supercapacitors with enhanced capacitances. ACS Nano 9(7):7563-7571

[9] Zheng W, Lv R, Na B, Liu H, Jin T, Yuan D (2017) Nanocellulose-mediated hybrid polyaniline electrodes for high performance flexible supercapacitors. J Mater Chem A 5(25):12969-12976

[10] Bhandari S, Khastgir D (2015) Synergistic effect of simultaneous dual doping in solvent-free mechanochemical synthesis of polyaniline supercapacitor comparable to the composites with multiwalled carbon nanotube. Polymer 81:62-69

[11] Bhandari S, Singha NK, Khastgir D (2013) Electrochemical synthesis of nanostructured polyaniline: heat treatment and synergistic effect of simultaneous dual doping. J Appl Polym Sci 129(3):1264-1273

[12] MacDiarmid AG, Epstein AJ (1995) Secondary doping in polyaniline. Synth Met 69(1):85-92

[13] Yin W, Ruckenstein E (2000) Soluble polyaniline co-doped with dodecyl benzene sulfonic acid and hydrochloric acid. Synth Met 108(1):39-46

[14] Bavio MA, Acosta GG, Kessler T (2014) Synthesis and characterization of polyaniline and polyaniline-Carbon nanotubes nanostructures for electrochemical supercapacitors. J Power Sources 245:475-481

[15] Singu BS, Srinivasan P, Pabba S (2011) Benzoyl peroxide oxidation route to nano form polyaniline salt containing dual dopants for pseudocapacitor. J Electrochem Soci, 159.

[16] Palaniappan S, Devi SL (2008) Novel chemically synthesized polyaniline electrodes containing a fluoroboric acid dopant for supercapacitors. J Appl Polym Sci 107(3): 1887-1892

[17] Arenas MC, Andablo E, Castaho VM (2010) Synthesis of conducting polyaniline nanofibers from single and binary dopant agents. J Nanosci Nanotechnol 10(1):549-554

[18] Stejskal J, Gilbert RG (2002) Polyaniline. Preparation of a conducting polymer(IUPAC technical report). Pure Appl Chem 74(5):857-867

[19] Ma Z, Shi W, Yan K, Pan L, Yu G (2019) Doping engineering of conductive polymer hydrogels and their application in advanced sensor technologies. Chem Sci 10(25):6232-6244

[20] Gawli Y, Banerjee A, Dhakras D, Deo M, Bulani D, Wad-gaonkar P, Shelke M, Ogale S (2016) 3D polyaniline architecture by concurrent inorganic and organic acid doping for superior and robust high rate supercapacitor performance. Sci Rep 6:21002

[21] Bautkinová T, Sifton A, Kutorglo EM, Dendisova M, Kopecký D, Ulbrich P, Mazúr P, Laachachi A, Hassouna F (2020) New approach for the development of reduced graphene oxide/polyaniline nanocomposites via sacrificial surfactant-stabilized reduced graphene oxide. Colloids Surf, A Phys Eng Aspects 589:124415

[22] Besbes I, Alila S, Boufi S (2011) Nanofibrillated cellulose from TEMPO-oxidized eucalyptus fibres: effect of the carboxyl content. Carbohyd Polym 84(3):975-983

[23] Trchová M, Morávková Z, Bláha M, Stejskal J (2014) Raman spectroscopy of polyaniline and oligoaniline thin films. Electrochim Acta 122:28-38

[24] Furukawa Y, Ueda F, Hyodo Y, Harada I, Nakajima T, Kawagoe T (1988) Vibrational spectra and structure of polyaniline. Macromolecules 21(5):1297-1305

[25] Jeon JW, Ma Y, Mike JF, Shao L, Balbuena PB, Lutkenhaus JL (2013) Oxidatively stable polyaniline:polyacid electrodes for electrochemical energy storage. Phys Chem Chem Phys 15(24):9654-9662

[26] Vallés C, Jiménez P, Muñoz E, Benito AM, Maser WK (2011) Simultaneous reduction of graphene oxide and polyaniline: doping-assisted formation of a solid-state charge-transfer complex. J Phys Chem C 115(21): 10468-10474

[27] Cho S, Lee JS, Jun J, Kim SG, Jang J (2014) Fabrication of water-dispersible and highly conductive PSS-doped PANI/-graphene nanocomposites using a high-molecular weight PSS dopant and their application in H2S detection. Nanoscale 6(24):15181-15195

[28] Pouget JP, Jozefowicz ME, Epstein AJ, Tang X, MacDiar-mid AG (1991) X-ray structure of polyaniline. Macromolecules 24(3):779-789

[29] French AD (2013) Idealized powder diffraction patterns for cellulose polymorphs. Cellulose 21(2):885-896

[30] Kutorglo EM, Hassouna F, Beltzung A, Kopecky D, Sedlarova I, Soóš M (2019) Nitrogen-rich hierarchically porous polyaniline-based adsorbents for carbon dioxide (CO2) capture. Chem Eng J 360:1199-1212

[31] Zhang X, Zhu J, Haldolaarachchige N, Ryu J, Young DP, Wei S, Guo Z (2012) Synthetic process engineered polyaniline nanostructures with tunable morphology and physical properties. Polymer 53(10):2109-2120

[32] Chen S-A, Lee H-T (1994) (1994) Structure and properties of poly(acry1ic acid)-doped polyaniline. Macromolecules 28:2858-2866

[33] Arsov LD, Plieth W, KoBmehl G (1998) Electrochemical and Raman spectroscopic study of polyaniline; influence of the potential on the degradation of polyaniline. J Solid State Electrochem 2(5):355-361

[34] Costentin C, Porter TR, Saveant J-M (2017) How do pseudocapacitors store energy? theoretical analysis and experimental illustration. ACS Appl Mater Interfaces 9(10): 8649-8658

[35] Posadas D, Rodriguez Presa MJ, Florit MI (2001) Apparent formal redox potential distribution in electroactive ary-lamine-derived polymers. Electrochim Acta 46(26): 4075-4081

[36] Motheo AJ, Santos JR, Venancio EC, Mattoso LHC (1998) Influence of different types of acidic dopant on the electrodeposition and properties of polyaniline films. Polymer 39(26):6977-6982

[37] Li X (2009) Improving the electrochemical properties of polyaniline by co-doping with titanium ions and protonic acid. Electrochim Acta 54(24):5634-5639

[38] Nekrasov AA, Gribkova OL, Ivanov VF, Vannikov AV (2010) Electroactive films of interpolymer complexes of polyaniline with polyamidosulfonic acids: advantageous features in some possible applications. J Solid State Elec-trochem 14(11):1975-1984

[39] Tarver J, Yoo JE, Dennes TJ, Schwartz J, Loo Y-L (2009) Polymer acid doped polyaniline is electrochemically stable beyond pH 9. Chem Mater 21(2):280-286

[40] Zhang X, Zhang H, Lin Z, Yu M, Lu X, Tong Y (2016) Recent advances and challenges of stretchable supercapacitors based on carbon materials. Sci China Mater 59(6): 475-494